

LAT Aerospace H2 Tech Meet

Team 58

Mathematical Modelling

Kuhn's Semi-Empirical Method

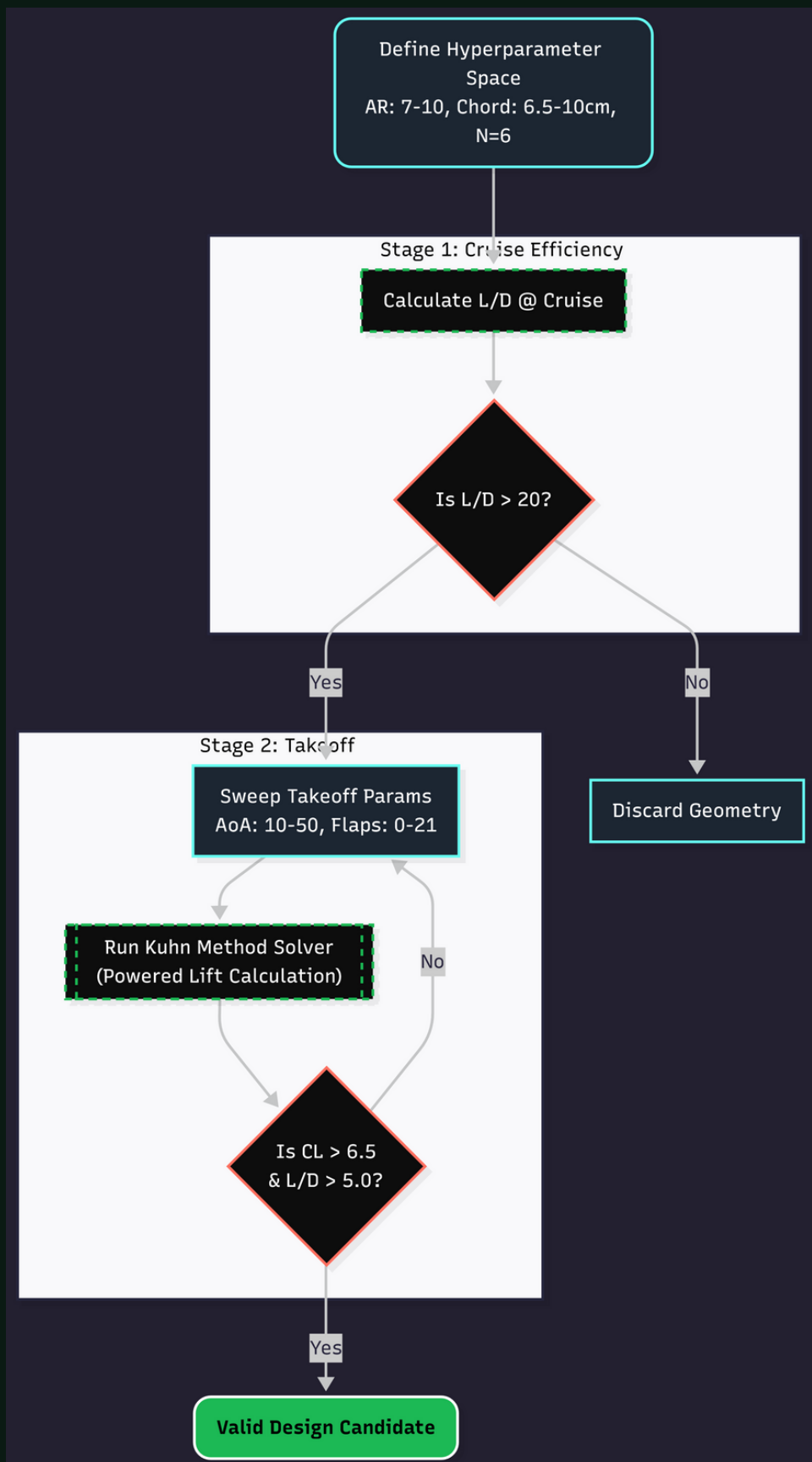
$$C_L = C_{L, off} + \sum_{n=1}^N \frac{F}{T} C_T'' \sin(\theta_n + \alpha_n) + \sum_{n=1}^N k \frac{F}{T} C_T'' \sin(\theta_n + \alpha_n) \frac{1}{\sqrt{1 + \frac{C_T'' S}{S_p}}}$$

$$C_X = \sum_{n=1}^N \frac{F}{T} C_T'' \cos(\theta_n + \alpha_n) - C_{D, off} - \sum_{n=1}^N k \frac{F}{T} C_T'' [1 - \cos(\theta_n + \alpha_n)] \frac{1}{\sqrt{1 + \frac{C_T'' S}{S_p}}}$$

- **Model:** Adopted Richard E. Kuhn's model (NASA TN D-3584) to enable rapid iteration of 36,000+ geometries, avoiding the prohibitive computational cost of full CFD during conceptual sizing.
- **Design Utility:** Explicitly derived for propeller-driven configurations, the method accurately models the unique interaction between high-mass-flow propeller slipstreams and the wing structure.
- **Validation:** Validated against flight data from the Breguet 941 and wind tunnel experiments, demonstrating robust lift prediction capabilities for STOL operations.

Hyperparameter Study

- **Exploration Scale:** Executed a high-volume sweep of 36,000+ configurations, prioritizing high-lift generation using Kuhn's formulation.
- **Drag Modeling Limitation:** Reliance on power-off airfoil polars proved insufficient, failing to account for significant slipstream-induced skin friction and pressure drag. This omission led to artificially inflated Cruise Efficiency (L/D) predictions, rendering the initial cruise filter ineffective.
- **Design Selection:** Despite drag inaccuracies, the study successfully identified the optimal geometric family:
 - Aspect Ratio: 10 (Maximized induced efficiency).
 - Propulsion: 6 Propellers (Optimal disk loading balance).



Inverse Kuhn Sizing

- **Motivation:** While the hyperparameter sweep successfully filtered for optimal geometric families (e.g., AR=10, N=6), it remained a qualitative tool due to drag modeling limitations.

- **Inverse Formulation:** Mathematically inverted Kuhn's standard model: instead of predicting Lift from Geometry, we solved for Geometry (Wing Chord) given a Target Lift ($C_L = 8.0$).

Derived Implicit Sizing Equation

$$C_w^2 = \frac{T_{tot} \sin(\theta(c_w) + \alpha)}{q(AR)(C_L - C_{L, off})} \left(1 + \frac{k}{\sqrt{1 + \frac{4T_{tot}N}{q\pi(AR)^2 c_w^2}}} \right)$$

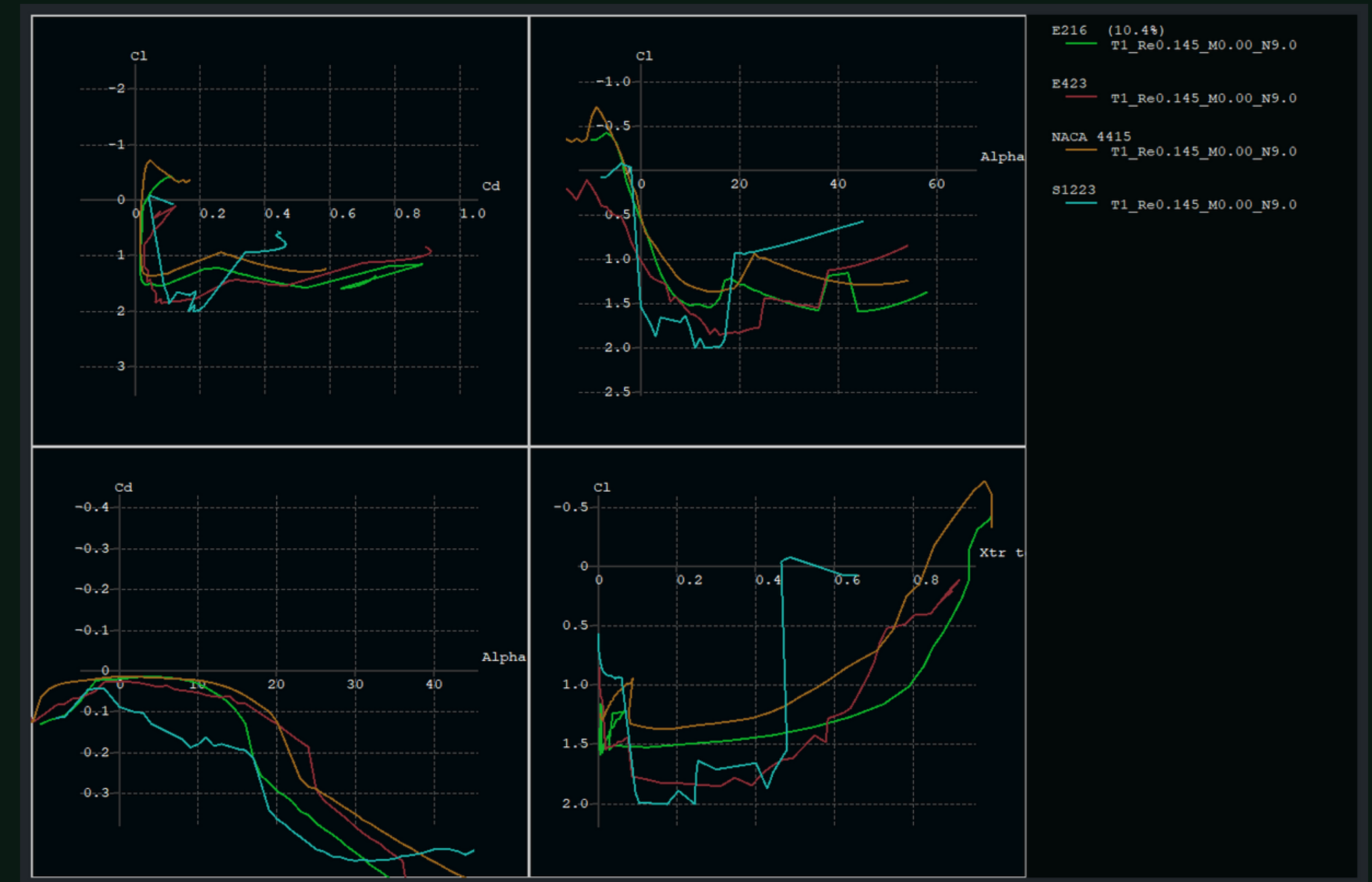
- **Result:** Analytically converged on a specific wing chord of $c_w = 0.096$ m. We finally got a initial starting point($AR= 10$, $N=6$, $C_f/C_w= 0.30$, $AoA @ Takeoff = 45deg$, $Flap_angle= 17.5deg$) for our CFD simulations.

Inverse Kuhn's Solver Results

Parameter	Value
Assumed Design Parameters	
Aspect Ratio (AR)	10
Number of Propellers (N)	6
Thrust per Propeller (APC Data)	12.5 N
Flap-to-Wing Chord Ratio (c_f/c_w)	0.30
Angle of Attack (α)	45°
Flap Deflection (δ_f)	17.5°
Target Lift Coefficient (C_L)	8.0
Freestream Velocity (V_∞)	20 m/s
Inverse Formulation Results	
Calculated Wing Chord (c_w)	0.0961 m
Verified (C_L) using direct Kuhn	8.48
Resulting Wing Span (b)	0.961 m
Total Thrust Required (T_{tot})	75.0 N

Airfoil Selection Criteria

- Highest lift coefficient among all evaluated airfoils at low Reynolds number.
- Best aerodynamic efficiency (C_L/C_D) in the operating regime.
- Smooth and delayed stall, enabling stable high-AoA operation.
- Validated through XFLR5 polars with consistent lift-drag behaviour.
- The Selig 1223 airfoil is found to be compatible with the Blown wing theory.



Design Overview

- **Geometry Setup:** 0.96 m span and 0.096 m chord.
- **Airfoil Choice:** Both root and tip use the Selig S1223 profile, enabled by a taper ratio of 1 for uniform aerodynamic behaviour.
- **Propulsion Layout:** Six 14 cm, 4-bladed propellers are distributed along the leading edge to ensure continuous slipstream coverage.
- **Propeller Placement:** Propellers set 2 cm aft of LE, 0.1 cm below chord.
- **Flaps:** single-slotted flap with flaperons at both ends, sized at 30% of chord

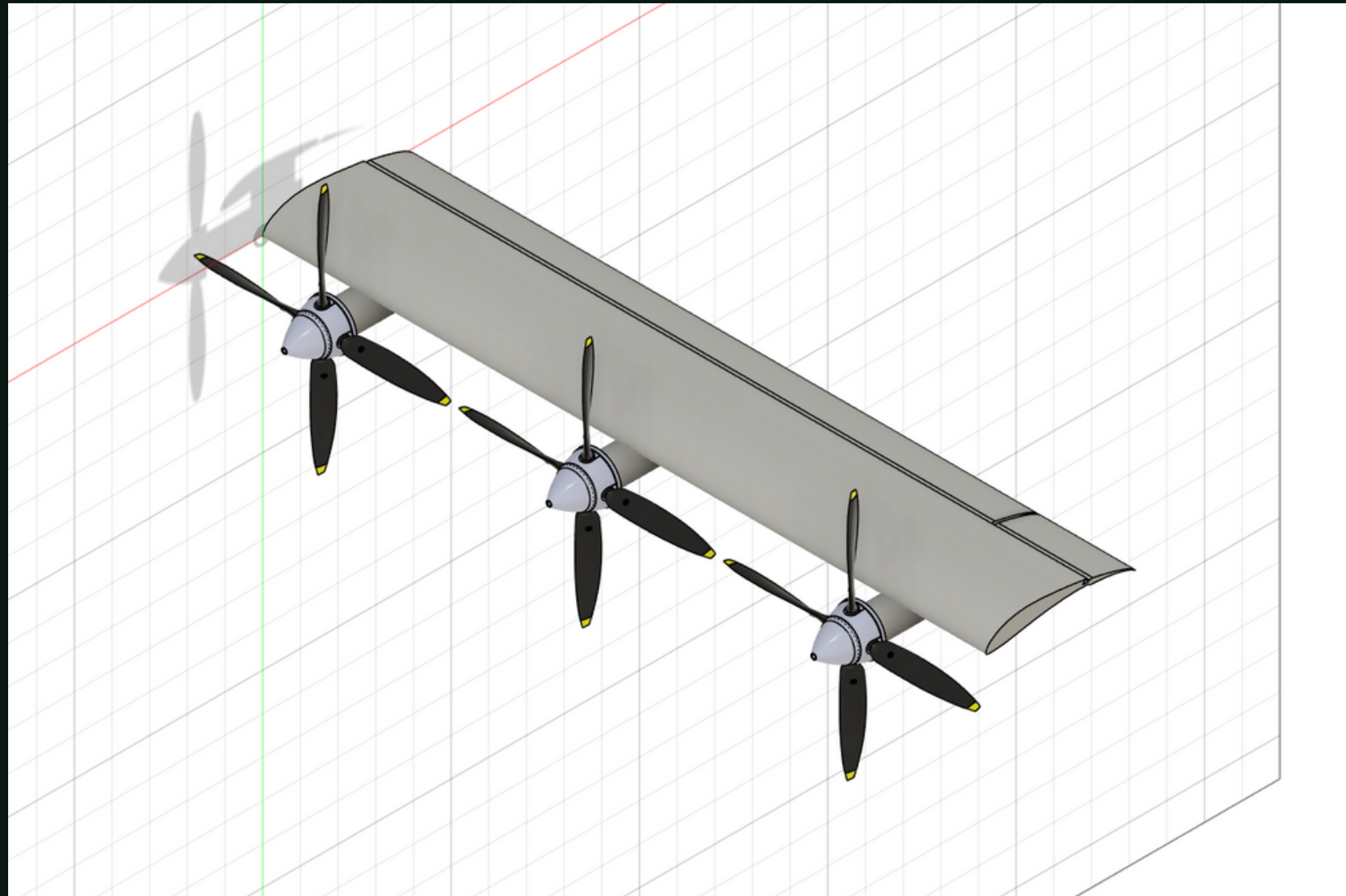


Fig : CAD model of half wing

Propeller Modelling

- APC (Advanced Precision Composites) provides detailed performance data for a wide range of propellers.
- Propeller size format: Diameter × Pitch (inches), e.g., 13×7E implies 13 in diameter, 7 in pitch, E = electric propeller
- Database includes only 2-bladed props
- Multi-bladed props are approximated by diameter scaling factors
 - 3-blade → multiply D by 0.90
 - 4-blade → multiply D by 0.84
- Design uses **six 4-Bladed Props of 14 cm diameter each**
- Therefore the 2-Bladed Prop Diameter, $D_2 = D_4 / 0.84 = 0.1666 \text{ m} = 6.56 \text{ in}$
- Closest APC match: **PER3_6×6E**
- Using $T/W = 0.65$ and $W = 15\text{Kg}$, Thrust per prop comes out to be **16 N**
- RPM required at takeoff $\approx 25000\text{-}26000$

Rankine-Froude Theory (Actuator Disc Modelling)

- Explicitly modelling rotating blades is computationally expensive.
- Actuator Disk Theory represents the propeller as a momentum-adding disk.
- Captures:
 - Induced velocities
 - Slipstream acceleration
 - Blown-wing interaction
- Significantly reduces computational cost while preserving thrust accuracy.

- Governing relation: $V_e = \sqrt{V_\infty^2 + \frac{2T}{\rho A}}$
- Computed Exit Velocities at
 - Takeoff = **45.8m/s** (Freestream Velocity = 20m/s)
 - Cruise = **87.6m/s** (Freestream Velocity = 80m/s)

CFD Methodology

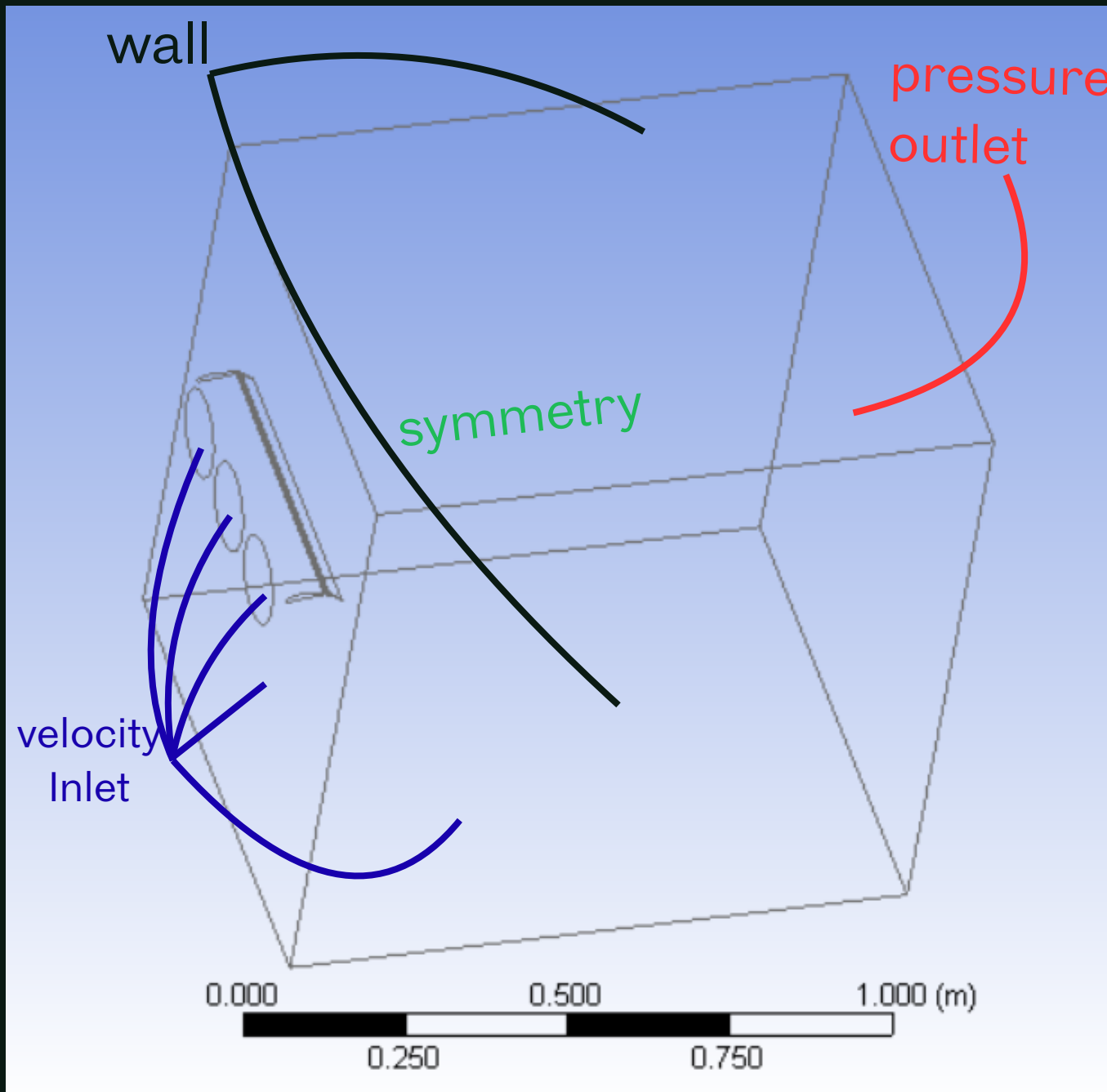
01 **GEOMETRY**

02 **MESH**

03 **MESH INDEPENDENCE AND
VALIDATION**

04 **SOLVER SETUP AND BOUNDARY
CONDITIONS**

Geometry



01

Geometry was created in ANSYS DesignModeler with parametric control for flap angle and propeller inlet location.

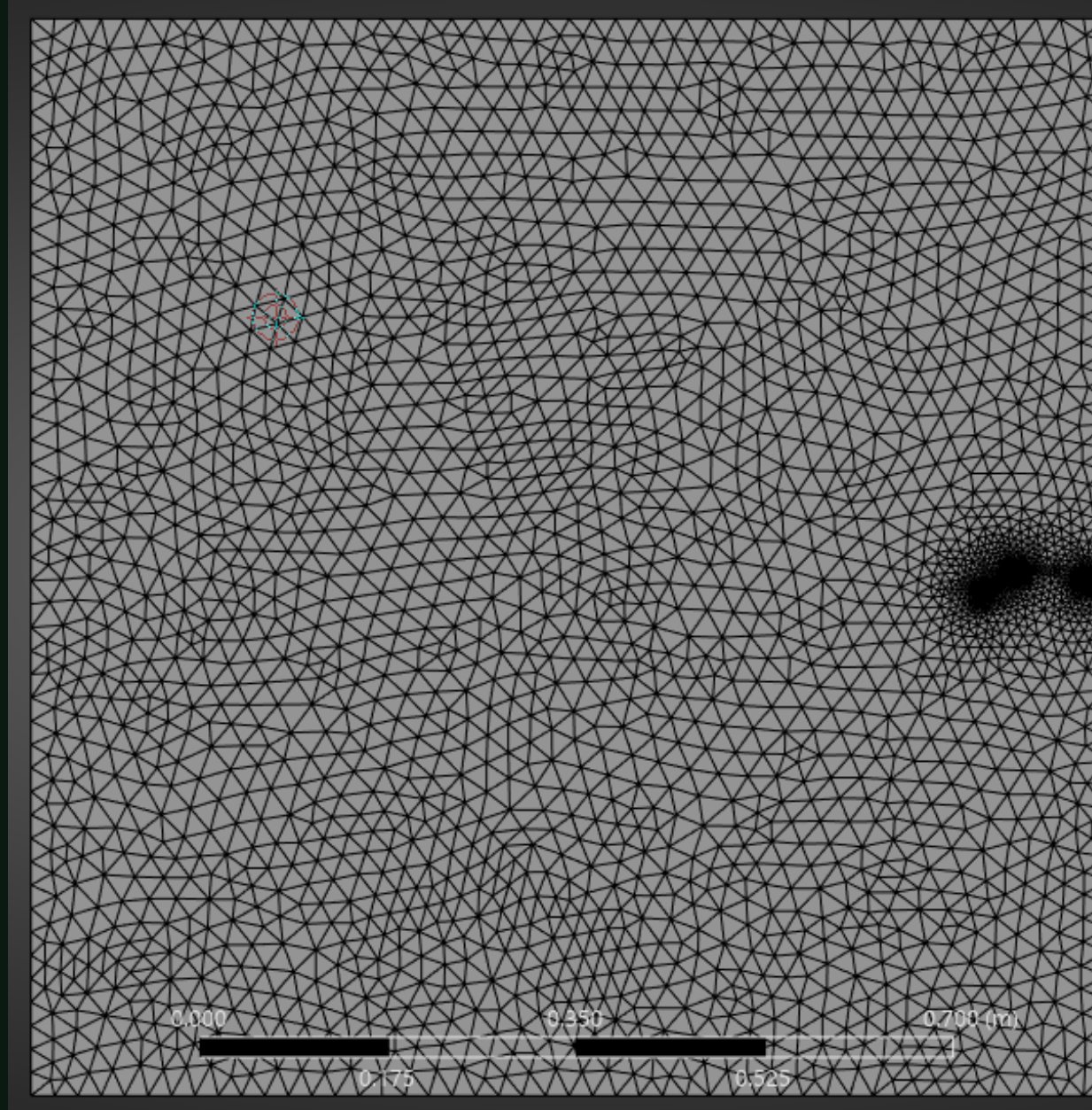
02

Wing and flap surfaces were modeled with precise chord length (0.096 m) and span (0.48 m) to match the actual configuration.

03

The domain dimensions were chosen large enough to avoid boundary interference.

Mesh



01

Meshing was performed in ANSYS Meshing using a tetrahedral mesh, suitable for capturing complex curvature and proximity around the wing–flap geometry.

02

A global element size of 22 mm was applied, with local refinement automatically generated around sharp edges and aerodynamic surfaces.

03

Final mesh statistics: $\approx 5,17,947$ nodes and $\approx 28,37,281$ elements

Mesh Independence

Mesh Quality	Element Size (mm)	Nodes	Elements	Lift Force (N)	Drag Force (N)	Percentage Error (%)
Coarse	22	517947	2837281	74.228	13.922	0 (reference)
Fine	8	1005493	5537052	74.239	13.928	0.0148 (Lift), 0.04309 (Drag)
Very Fine	2	3901557	22017579	73.865	13.782	0.4890 (Lift), 1.0056 (Drag)

01

Simulations were run on Coarse (2.8M elements), Fine (5.5M elements), and Very Fine (22M elements) meshes to assess sensitivity.

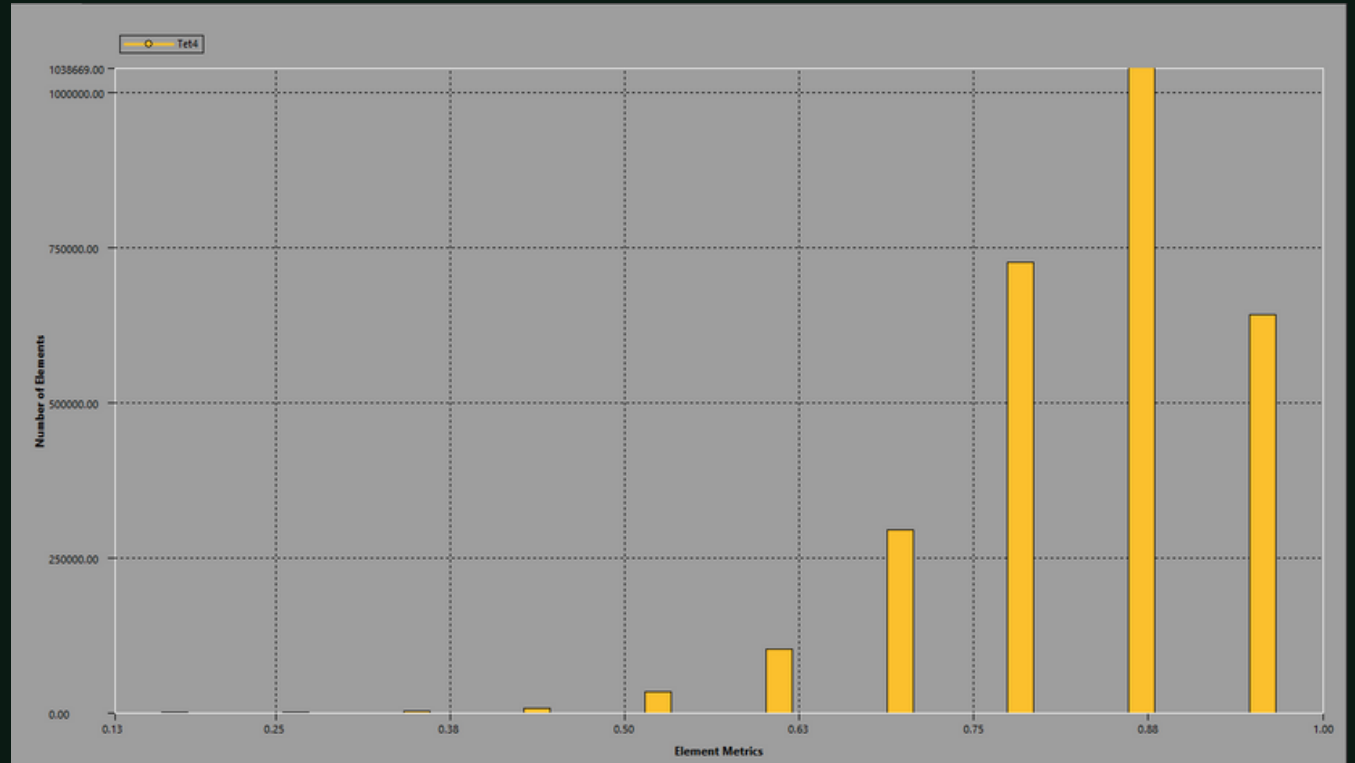
02

Lift and drag varied very little, with maximum errors of ~0.49% (Lift) and ~1.00% (Drag), confirming mesh independence.

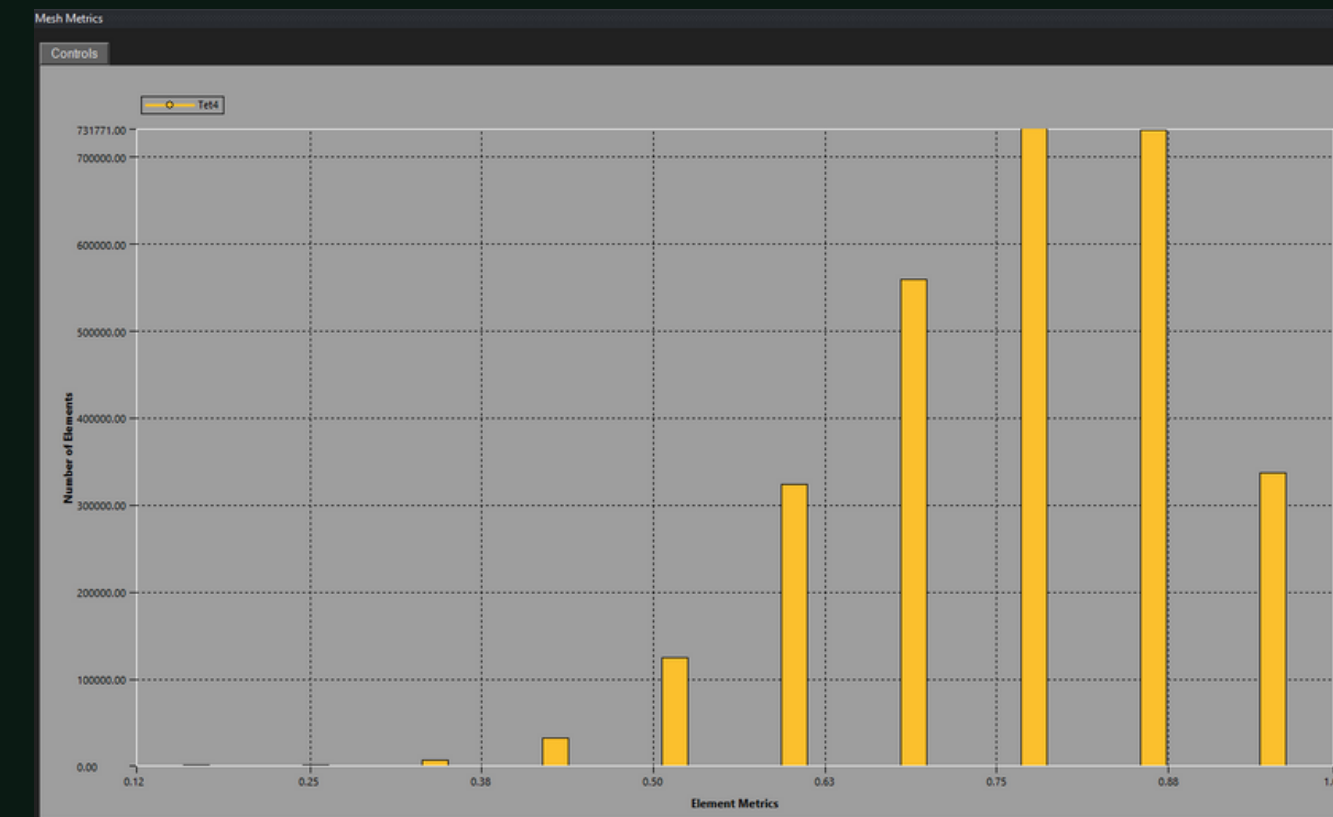
03

Due to negligible error change and limited computational power, the coarse mesh was selected for final CFD runs.

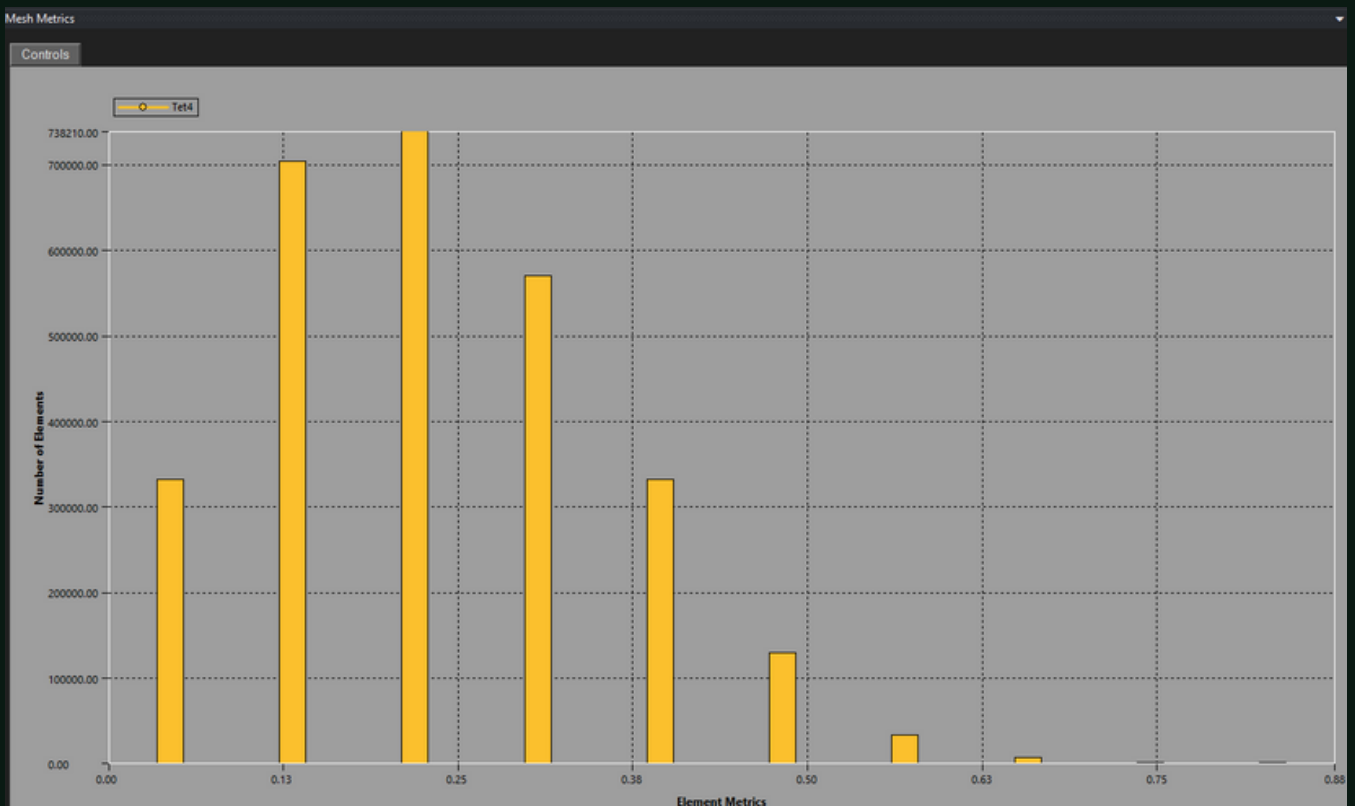
Mesh Validation



Element Quality mesh metric



Orthogonal Quality mesh metric



Skewness mesh metric

01 Quality metrics (Element Quality, Orthogonal Quality, Skewness) show most elements lie in the high-quality range.

02 Average orthogonal quality ≈ 0.76 , and skewness remains low, indicating stable numerical behaviour.

03 No highly distorted elements were observed, confirming the mesh is valid and suitable for accurate CFD analysis.

Solver Setup and Boundary Conditions

01 SOLVER SETUP

A steady-state pressure-based solver with SST k- ω turbulence model and second-order discretisation was used for accurate aerodynamic prediction.

02 BOUNDARY CONDITIONS:

Velocity inlet and propeller exit velocity were defined as parametric inputs, and the outlet was defined as a pressure outlet with 0Pa gauge pressure.

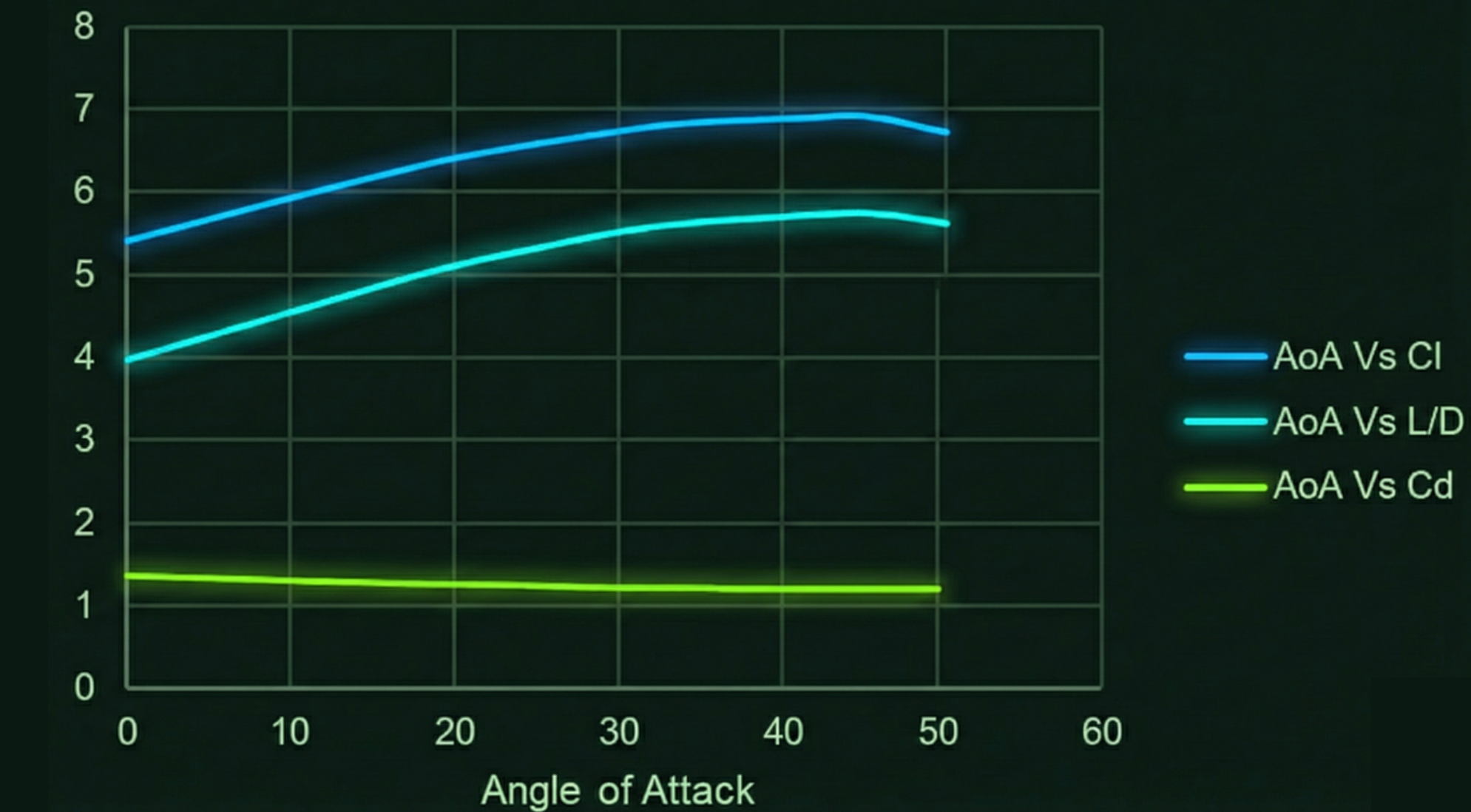
03 CONVERGENCE

Solution converged with continuity of 1×10^{-3} , and lift/drag plots becoming steady, indicating a stable steady-state solution.

Parametric Studies

#1. Study on Effect of Angle of Attack at Fixed Flap Deflection

AoA (°)	Flap (°)	L (N)	D (N)	CL	CD	L/D
0	17.5	121.878	30.712	5.398	1.36	3.969
10	17.5	133.652	29.36	5.919	1.3	4.552
20	17.5	144.556	28.246	6.402	1.251	5.118
30	17.5	151.956	27.524	6.73	1.219	5.523
35	17.5	154.444	27.34	6.84	1.211	5.648
40	17.5	155.254	27.17	6.876	1.203	5.713
45	17.5	156.05	27.1	6.911	1.2	5.759
50	17.5	151.618	26.908	6.715	1.192	5.633



- Obtained the highest lift at 45° AoA.

#2. Study on Effect of Flap Deflection at Optimal AoA = 45°

AoA (°)	Flap (°)	L (N)	D (N)	CL	CD	L/D
45	15	152.524	24.542	6.757	1.087	6.216
45	17.5	156.05	27.1	6.911	1.2	5.759
45	20	155.572	29.154	6.894	1.291	5.335

- Obtained the highest lift at 45° AoA and 17.5° flap deflection.

#3. Study on Propeller Vertical Location

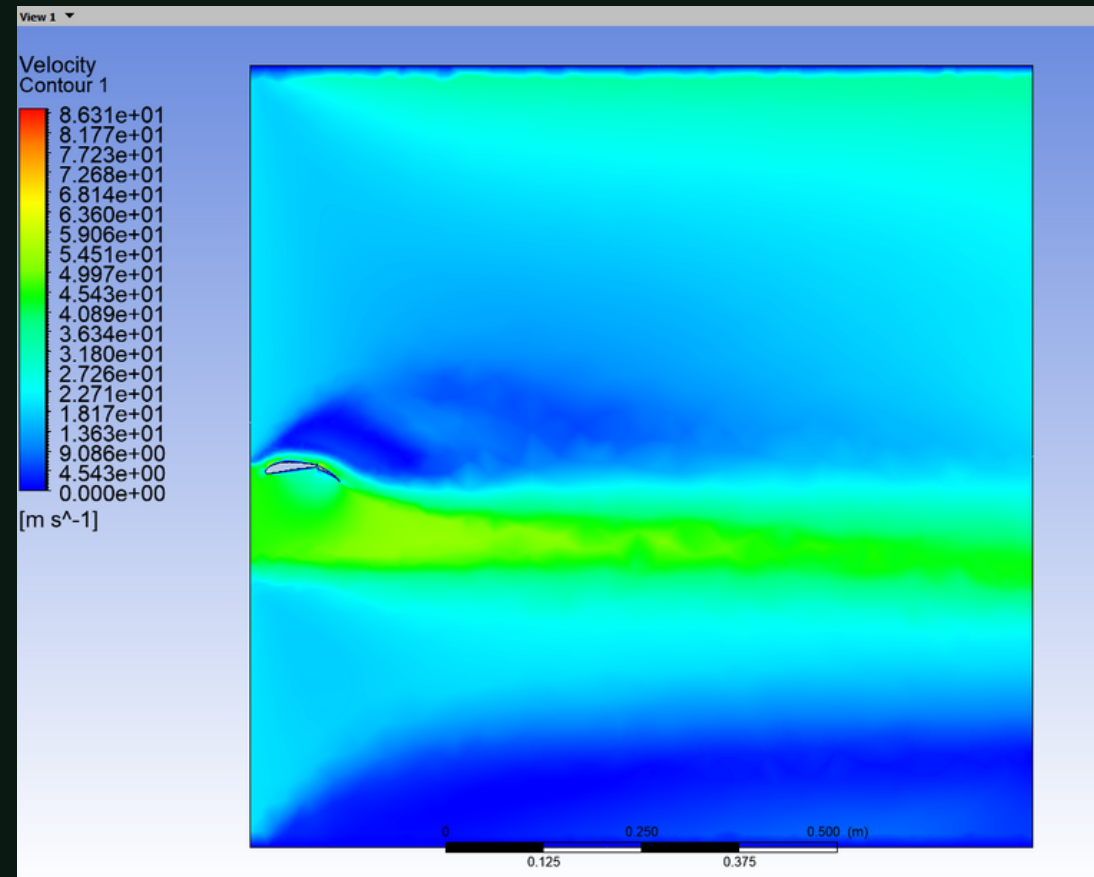
Quantitative study

AoA	Flap Deflection (°)	Lift Force (N)	Drag Force (N)	Prop_Vert (m)
45	17.5	47.744	2.229	0.06
45	17.5	67.03	9.57	0.03
45	17.5	78.025	13.55	0.001

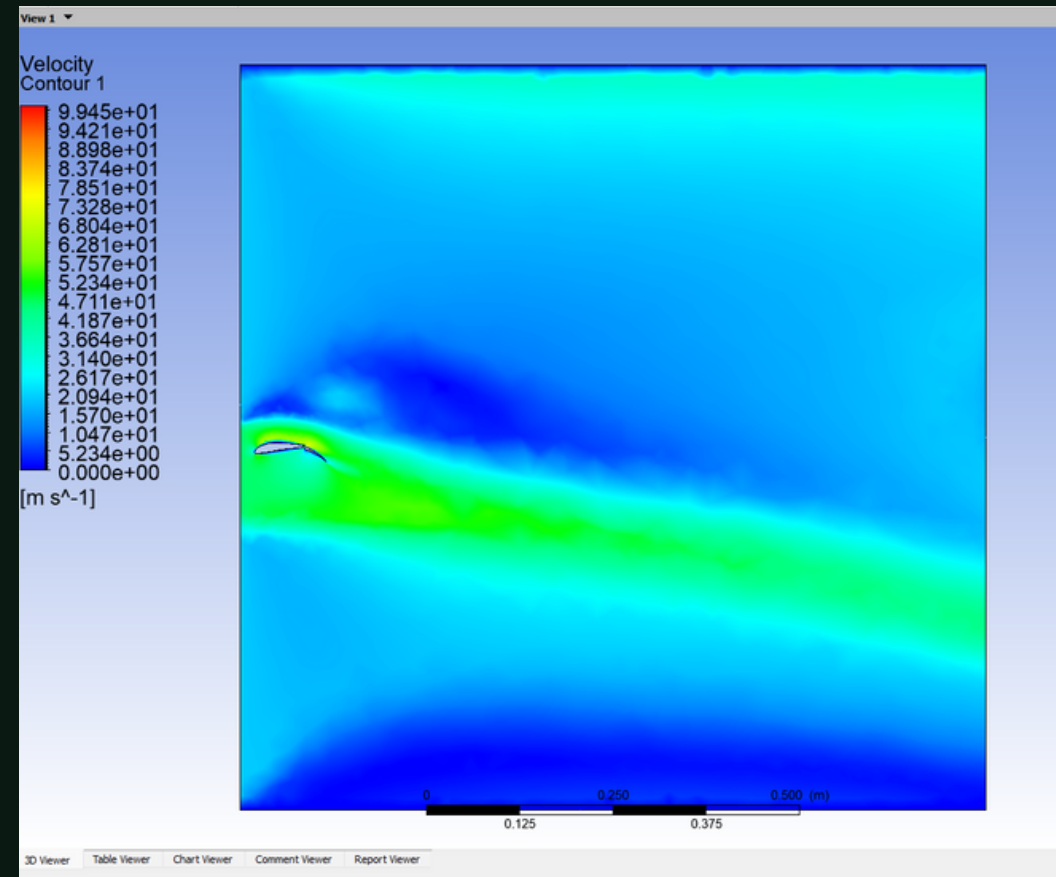
- Obtained the highest Lift force at 0.001m propeller vertical distance.
- As we moved the propeller closer to the wing, we observed an increased Lift force as well as increased parasite drag.
- We chose 0.001m prop_vert location, because it was the only geometry that met the lift requirement.

#3. Study on Propeller Vertical Location

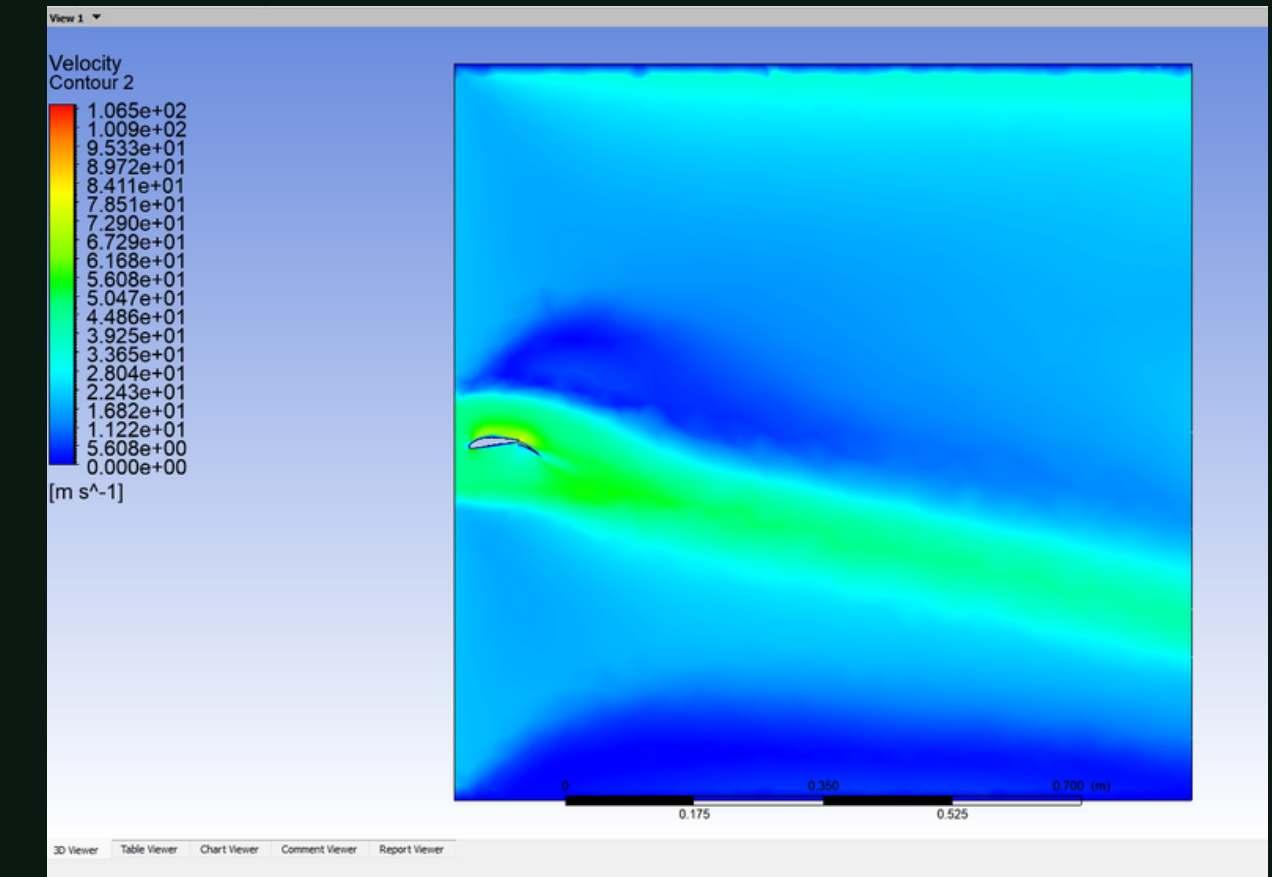
Qualitative study



Velocity field for propeller located 0.06 m below wing centreline. The jet remains largely undeflected and does not contribute significantly to lift.



Velocity field for propeller located 0.03 m below centreline.
Partial jet deflection increases circulation and lift.



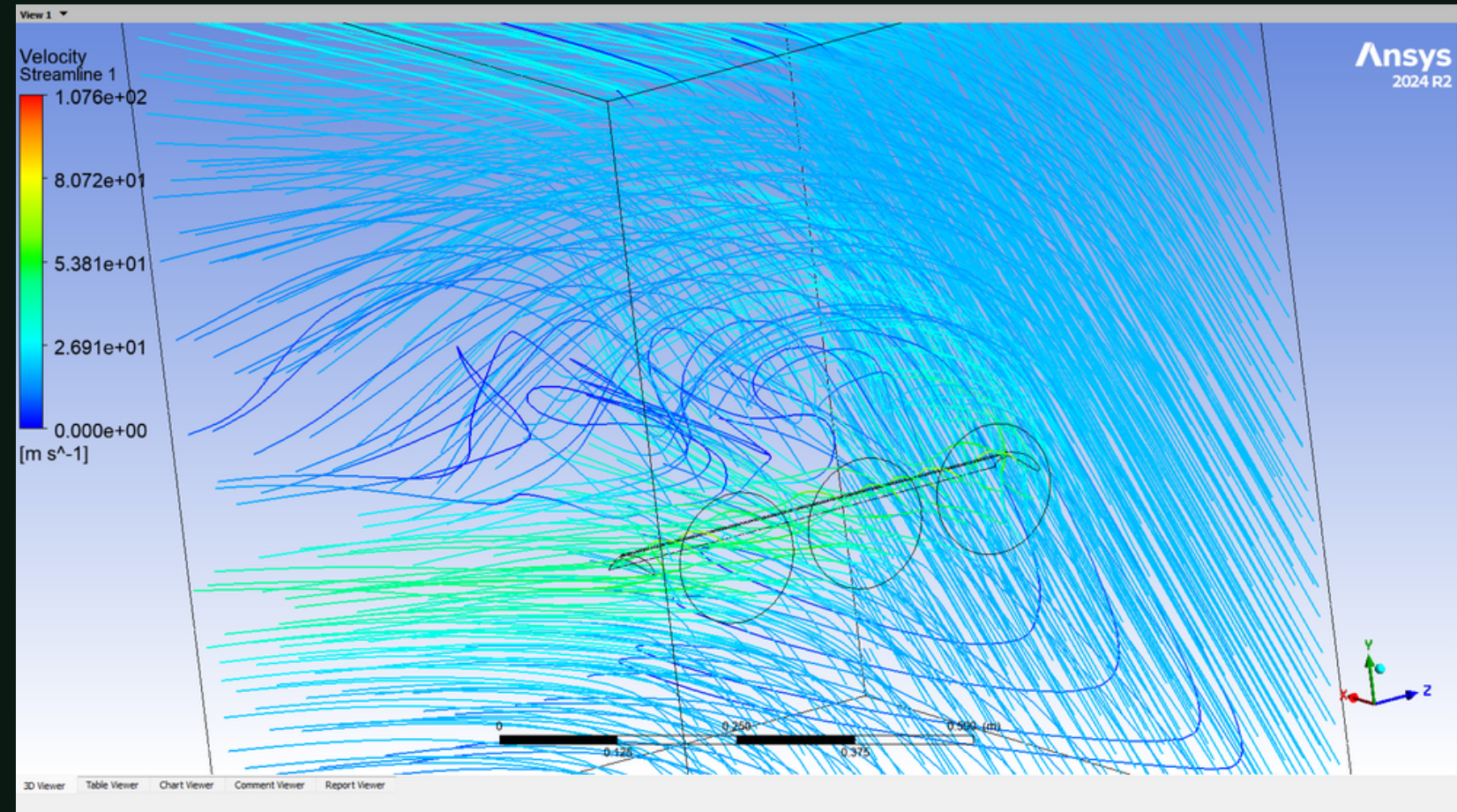
Velocity field for propeller located 0.001 m below centreline.
The slipstream fully attaches to the wing, producing maximum lift.

#4. Parametric Study for Cruise

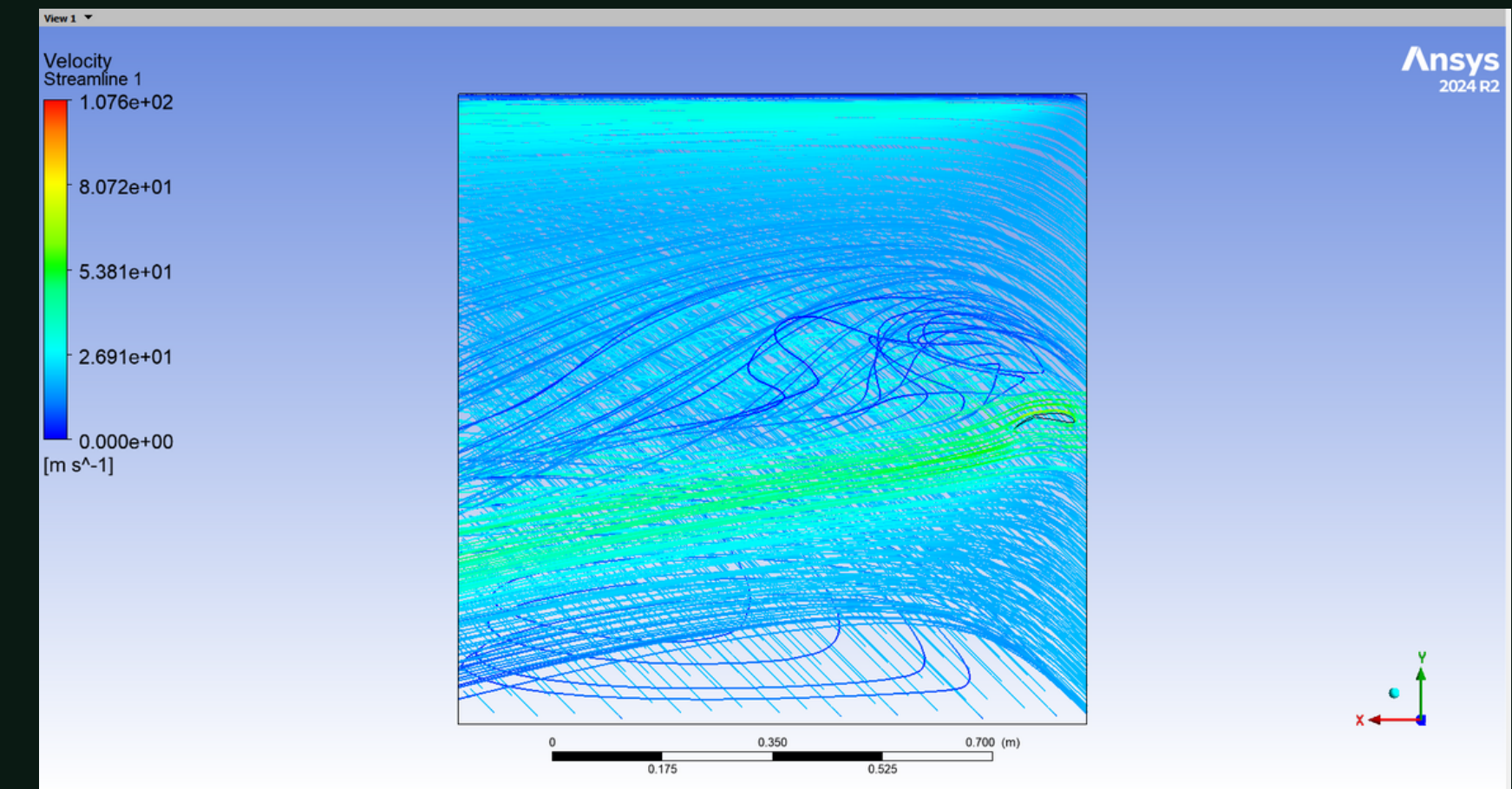
AoA (°)	Flap (°)	L (N)	D (N)	CL	CD	L/D
0	0	444.32	56.086	1.355	0.171	7.92
0	15	696.822	117.93	2.122	0.359	5.91

- Obtained the highest L/D at 0° AoA and 0° flap deflection.

Flowfield Visualisation #1

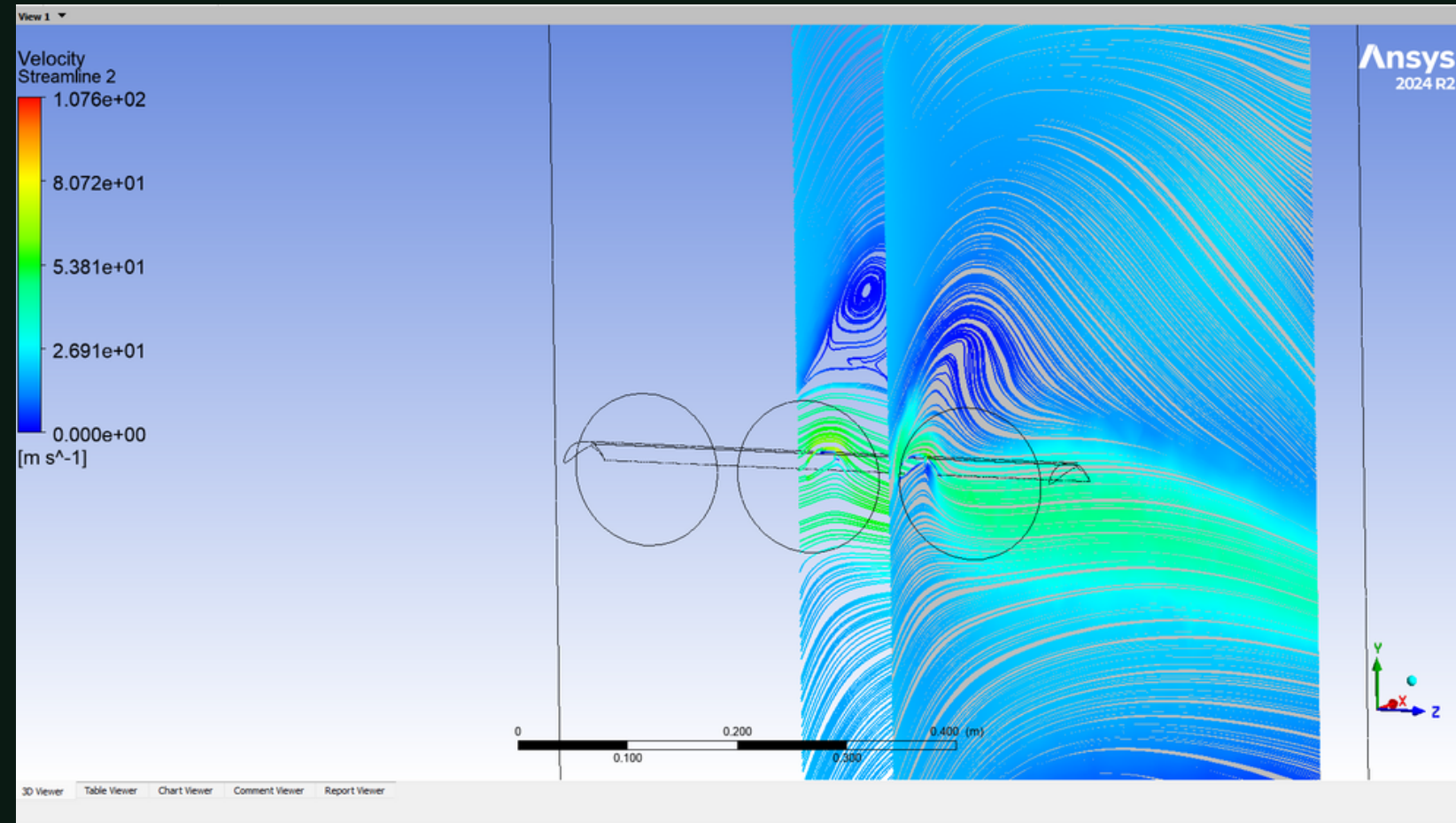


Three-dimensional streamlines showing slipstream attachment, jet curvature, and wake deflection.

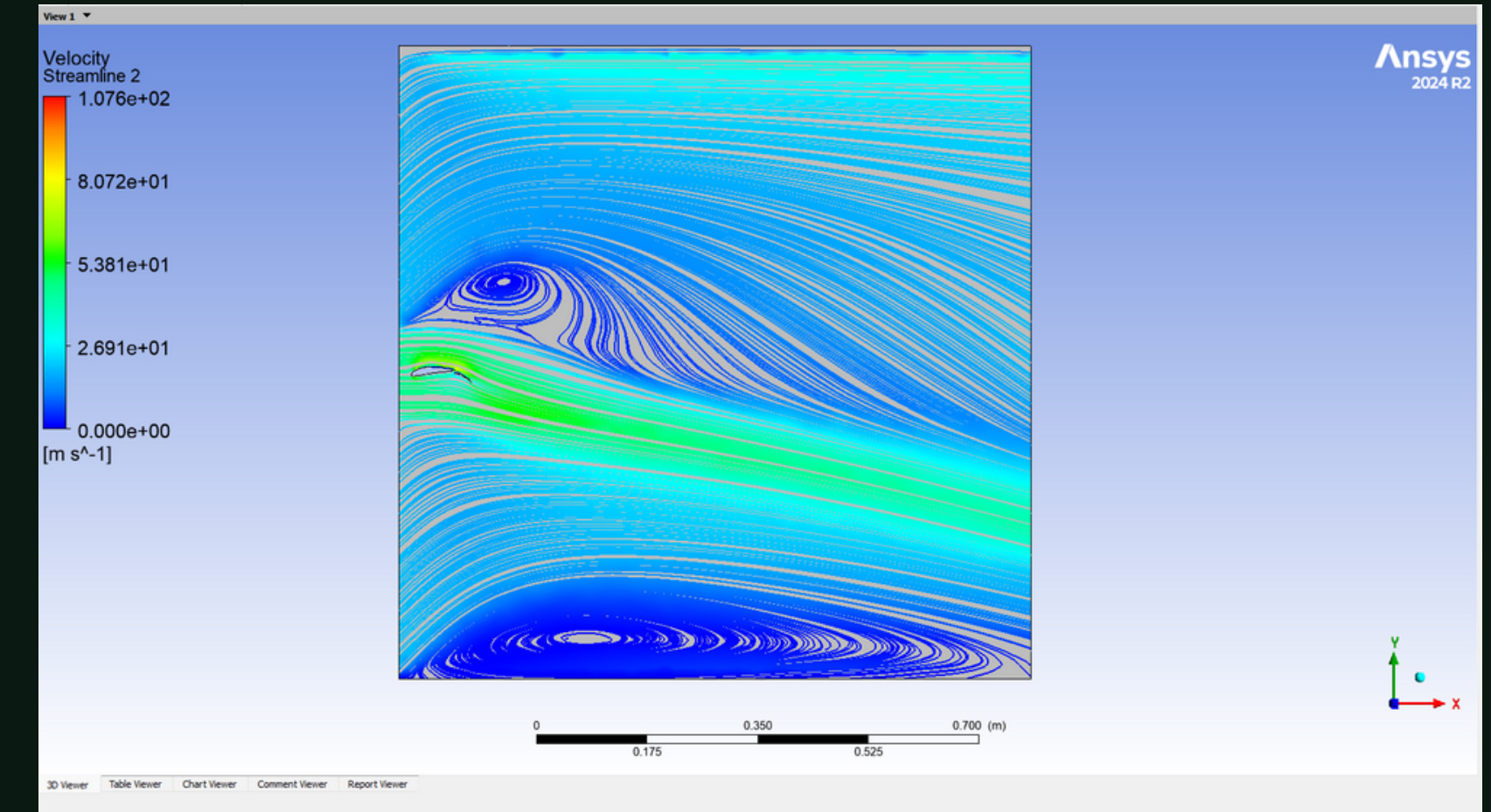


Side view of 3D streamlines showing slipstream adherence to the flap and downward jet deflection.

Flowfield Visualisation #2

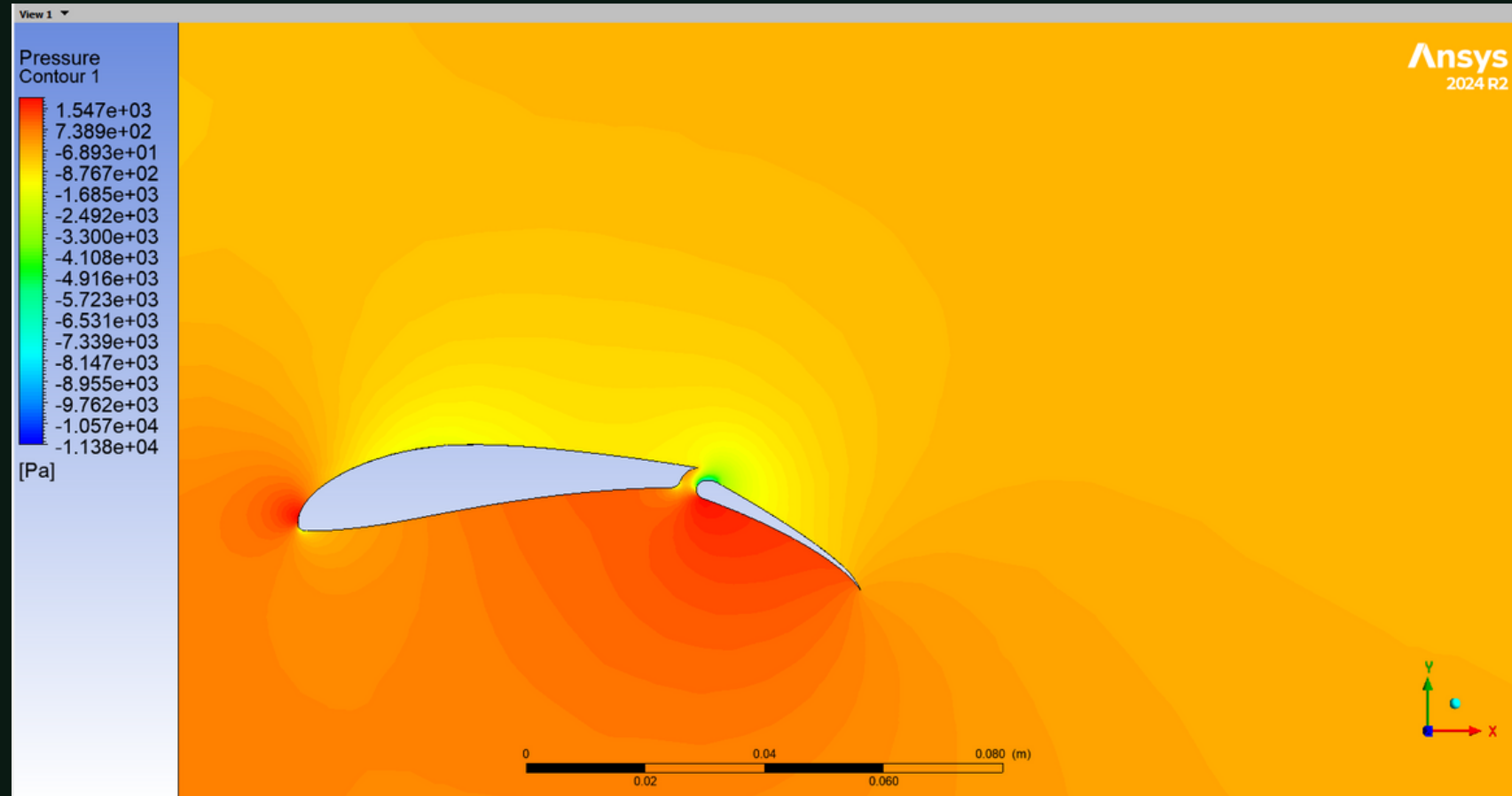


Streamlines at the two plane sections.

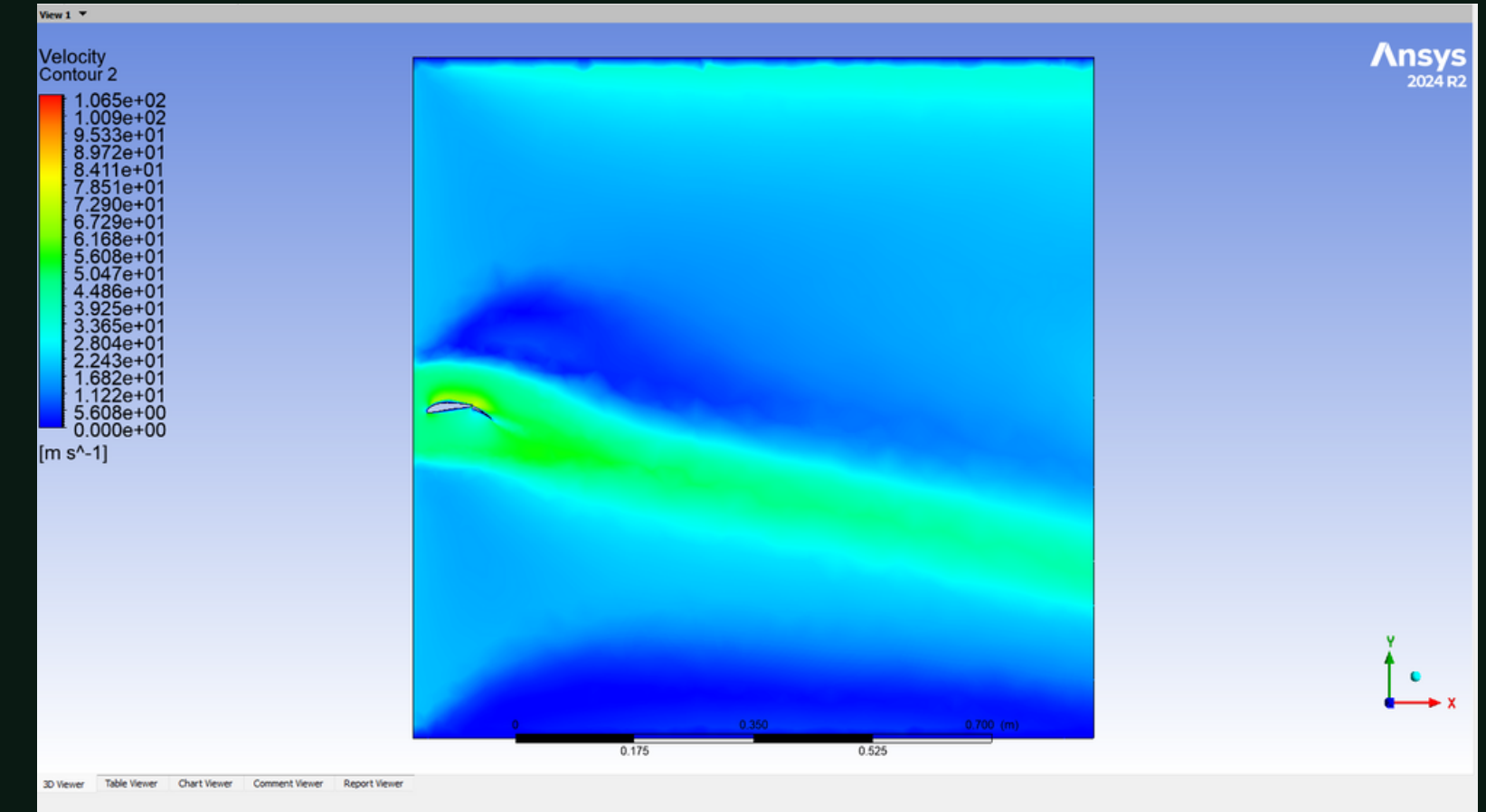


Mid-plane streamlines showing accelerated flow over the wing.

Flowfield Visualisation #3

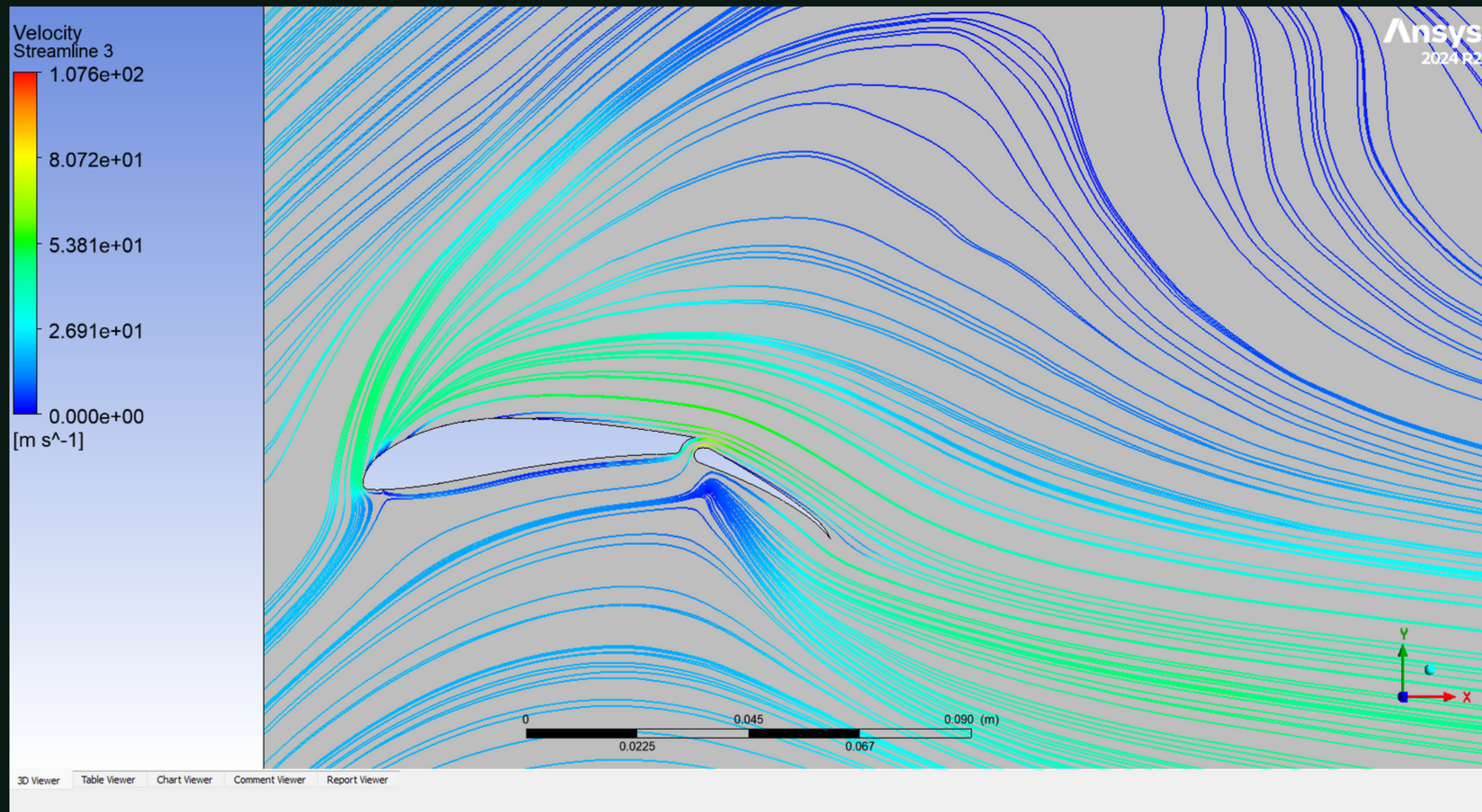


Pressure contour showing intense low-pressure region at the flap leading edge and large pressure gradient on the upper and lower surface of the airfoil.



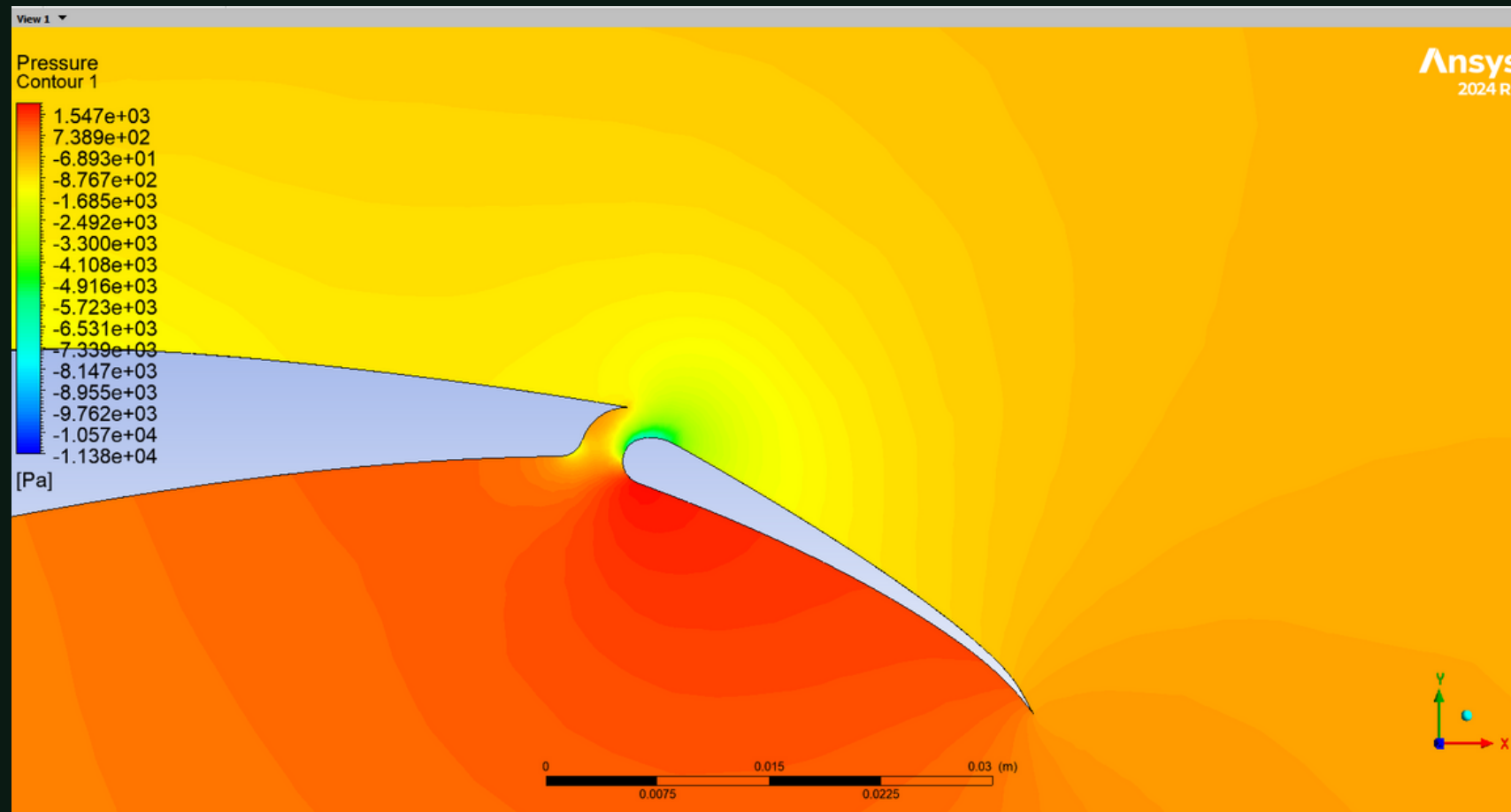
Downstream velocity field showing downward-deflected jet indicating powered-lift generation.

Flow Physics of the Slotted Flap #1

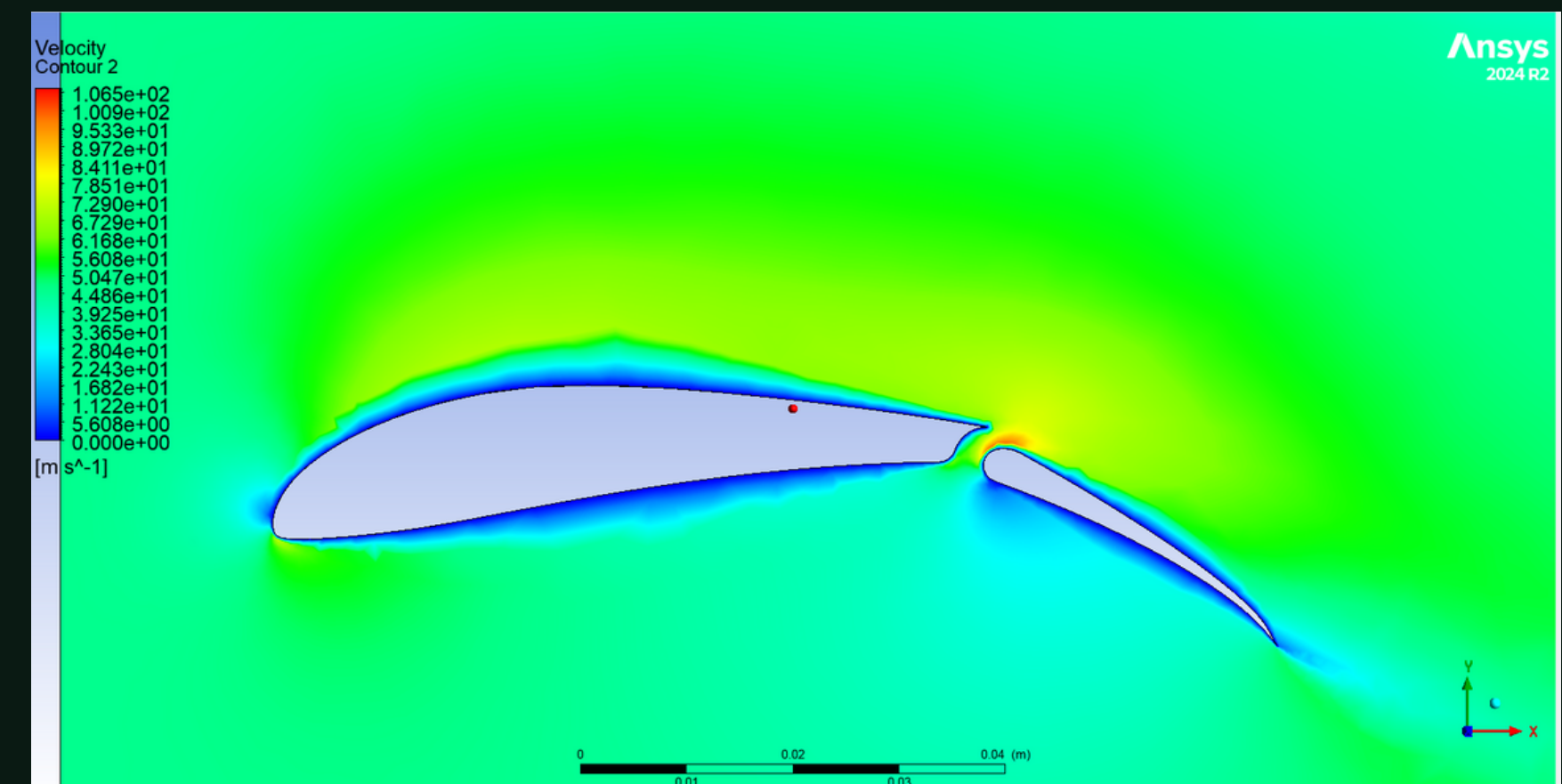


Streamlines passing through the slot and re-energizing
the flap boundary layer.

Flow Physics of the Slotted Flap #2



Zoomed-in pressure field showing the strong suction created by slot-induced reattachment.



Zoomed-in velocity field at the slot showing high-speed jet injection and flap reattachment.

Final Design Assessment

	AoA (°)	Flap Def (°)	CL	L/D
Takeoff	45	17.5	6.911	5.758
Cruise	0	0	1.355	7.92



